



**HAL**  
open science

# Modeling the Injection-Locked Behavior of a Quantum Dash Semiconductor Laser

Nader A. Naderi, Mike Pochet, Frédéric Grillot, Nathan B. Terry, Vassilios Kovanis, Luke F. Lester

► **To cite this version:**

Nader A. Naderi, Mike Pochet, Frédéric Grillot, Nathan B. Terry, Vassilios Kovanis, et al.. Modeling the Injection-Locked Behavior of a Quantum Dash Semiconductor Laser. IEEE Journal of Selected Topics in Quantum Electronics, 2010, 15 (3), pp.563-571. 10.1109/JSTQE.2009.2015334 . hal-00501876

**HAL Id: hal-00501876**

**<https://hal.science/hal-00501876>**

Submitted on 12 Jul 2010

**HAL** is a multi-disciplinary open access archive for the deposit and dissemination of scientific research documents, whether they are published or not. The documents may come from teaching and research institutions in France or abroad, or from public or private research centers.

L'archive ouverte pluridisciplinaire **HAL**, est destinée au dépôt et à la diffusion de documents scientifiques de niveau recherche, publiés ou non, émanant des établissements d'enseignement et de recherche français ou étrangers, des laboratoires publics ou privés.

# Modeling the Injection-Locked Behavior of a Quantum Dash Semiconductor Laser

Nader A. Naderi, *Student Member, IEEE*, Mike Pochet, Frédéric Grillot, *Member, IEEE*, Nathan B. Terry, Vassilios Kovanis, and Luke F. Lester, *Senior Member, IEEE*

**Abstract**—Using the conventional rate equations describing an injection-locked system, a novel modulation response function is derived, which implicitly incorporates nonlinear gain through the free-running relaxation oscillation frequency and damping rate of the slave laser. In this paper, it is shown that the model presented can be used to extract the characteristic parameters of the coupled system from experimental data. The number of fitting parameters in the model is reduced by determining the fundamental slave parameters through the conventional free-running response function; these parameters are considered to be constant during the curve-fitting of the injection-locked system. Furthermore, in order to reduce the number of possible solutions generated during the least-squares-fitting process, the remaining fitting parameters are tightly constrained based on the physical limits of the coupled system. By reducing the number of unknown fitting parameters and constraining the remaining terms, a stronger confidence in the extracted parameters is achieved. Using a series of response curves measured from an injection-locked quantum dash laser, characteristic parameters of the system are extracted and validity of the model is examined. The verified model is used to analyze the impact of the linewidth enhancement factor on the characteristics of the response function in the microwave domain.

**Index Terms**—High-speed modulation, injection-locking, quantum dash, semiconductor laser.

## I. INTRODUCTION

INJECTION-locking of semiconductor lasers is one of the most attractive research topics since this method induces superior improvement in the high-speed characteristics of directly modulated lasers such as increasing the modulation bandwidth, suppressing nonlinear distortion, relative intensity noise, mode hopping, and reducing chirp [1]–[7]. Previous work has focused on realizing high modulation bandwidths and associated design strategies, analyzed the modulation properties of the coupled system in the spectral domain, and numerically investigated the modulation response of the injection-locked system [4]–[11].

Noting the benefits of extracting relevant operating parameters from measured data in order to aid in future simulations, this paper focuses on extracting the operating parameters from

an injection-locking system by introducing a novel modulation response function and experimentally verifying the validity of the resultant model in the microwave domain using a quantum dash (QDash) Fabry–Perot (FP) device as the slave laser. The extracted parameters of the coupled injection-locked system include the injection strength, linewidth enhancement factor, threshold gain shift, coupled phase offset between the master and slave laser, and the field enhancement factor that characterizes the deviation of the locked slave laser from its free-running value. This paper theoretically shows how the derived model incorporates nonlinear gain through the free-running damping rate and relaxation oscillation frequency, along with the impact of nonlinear gain compression for the QDash FP device under investigation, thereby accounting for the unique properties introduced by quantum dot physics. The validity of the model and accuracy of extracted terms are examined based on theoretically expected values for the fitting parameters at extreme detuning ranges. Lastly, the derived model is used to perform theoretical simulations to analyze the impact of the linewidth enhancement factor on the characteristics of the modulation response function.

## II. THEORETICAL MODEL

In order to understand the limiting factors in an injection-locked system, it is important to investigate the governing theory that can be obtained by modeling the characteristic parameters using a set of coupled rate equations [12]–[14]. Mathematical translation of the injection-locking system operating in the stable locking regime based on three fundamental rate equations was first demonstrated by Lang [12]. This paper capitalizes on improvements to the rate equations governing the dynamic properties of an injection-locked system in order to investigate the modulation properties of such a system under strong injection [8]–[10].

### A. Rate Equations

The differential equations describing the dynamics of an injection-locked system have been developed by introducing terms describing the impact of optical injection to the conventional rate equations governing the free-running characteristics of the slave laser. The additional terms include a coupling value  $k_c$ , the magnitude of the injected master field  $A_{inj}$ , and the detuning frequency between master and slave  $\Delta\omega_{inj}$ . The model assumes the slave laser is being directly modulated such that the small-signal approximation can be applied. Additionally, it is assumed that the laser has been exposed to a relatively strong external optical injection, such that the impact of the noise and

Manuscript received November 1, 2008; revised January 24, 2009. First published May 12, 2009; current version published June 5, 2009. This work was supported by the U.S. Air Force Research Laboratory under Grant FA8750-06-1-0085. The work of N. Terry and V. Kovanis was supported by Air Force Office of Scientific Research (AFOSR) Laboratory Research Initiation Request (LRIR) 09RY04COR.

N. A. Naderi, M. Pochet, F. Grillot, and L. F. Lester are with the Center for High Technology Materials, University of New Mexico, Albuquerque, NM 87106 USA (e-mail: nader@chtm.unm.edu; mpochet@unm.edu; fgrillot@chtm.unm.edu; luke@chtm.unm.edu).

N. Terry and V. Kovanis are with the US Air Force Research Laboratory, 2241 Avionic Circle, Wright-Patterson Air Force Base (WPAFB), OH 45433 USA (e-mail: nathan.terry@wpafb.af.mil; vassilios.kovanis@wpafb.af.mil).

Digital Object Identifier 10.1109/JSTQE.2009.2015334

the spontaneous emission rate coupled to the lasing mode are negligible [10]. The free-running FP slave laser has cleaved facets and is biased well above threshold. As in the free-running case, the amplitude and phase equations arise from the fundamental complex field rate equation. The variation of the slave field magnitude, phase offset between the master and slave fields and carrier density with time can be written as [8], [10]:

$$\frac{dA}{dt} = \left(\frac{g}{2}\Delta N\right) A + (k_c \cos \phi) A_{\text{inj}} \quad (1)$$

$$\frac{d\phi}{dt} = \alpha \left(\frac{g}{2}\Delta N\right) - \Delta\omega_{\text{inj}} - (k_c \sin \phi) \frac{A_{\text{inj}}}{A} \quad (2)$$

$$\frac{dN}{dt} = J_{\text{bias}} - \gamma_N N - (\gamma_P + g\Delta N) A^2 \quad (3)$$

where  $A$  is the internal slave's amplitude of the electric field,  $g$  is the differential gain,  $N$  is the carrier density, and  $\Delta N = N - N_{\text{th}}$  is the shift in carrier density from the threshold.  $\phi$  is the phase offset between master and slave laser, which is defined as  $\phi_{\text{slave}} - \phi_{\text{master}}$ , the amplitude of the electric field square  $A^2$  is proportional to photon density  $P$ , and  $J_{\text{bias}}$ ,  $\gamma_N$ ,  $\gamma_P$  correspond to the applied bias current density, inverse differential carrier lifetime, and photon decay rates, respectively. It is important to note that the phase variation in time depends on detuning through  $\Delta\omega_{\text{inj}} = \omega_{\text{slave}} - \omega_{\text{master}}$ . The linewidth enhancement factor  $\alpha$ , injection strength, which is proportional to  $A_{\text{inj}}/A$ , phase offset  $\phi$ , and detuning term  $\Delta\omega_{\text{inj}}$  are the key and defining injection parameters that have a significant impact on the coupled oscillator system.

### B. Steady-State Solutions

The equations described in (1)–(3) define the temporal and dynamic behavior of the system. The injection-locking phenomenon is investigated through the steady-state solutions arising from these three differential equations. Under steady-state, the right hand side of (1)–(3) is equal to zero as there will be no time variation in the slave's field amplitude, phase, and carrier density. Using an approach presented by Murakami *et al.* [8], the steady-state parameters of the injection-locked system can be defined as the steady-state phase offset  $\phi_0$ , steady-state carrier density  $N_0$ , steady-state locked slave field  $A_0$ , and the free-running slave field  $A_{fr}$  [10]. Based on this strategy, the first general condition for the system under injection locking can be clearly found through (2) by introducing the steady-state parameters and setting the left hand side equal to zero:

$$\Delta\omega_{\text{inj}} = \frac{\alpha}{2} (g\Delta N_0) - (k_c \sin \phi_0) \frac{A_{\text{inj}}}{A_0} \quad (4)$$

where the change in carrier density under steady-state condition is expressed as  $\Delta N_0 = N_0 - N_{\text{th}}$ . Note that for stability, it is required that the change in the steady-state carrier density be less than zero  $\Delta N_0 < 0$ . Equation (4) describes the correlation between frequency detuning, threshold condition, and the strength of the injected field. It can be clearly seen that depending on the detuning condition and the phase offset, the injected field can result in a threshold gain shift through  $g\Delta N_0$ . Note that the group velocity is implicit in the differential gain term  $g$ .

Using this method and solving the steady-state parameters of the coupled system, the relationship between the free-running and locked fields and also the expression for the steady-state phase offset can be expressed as [8], [10]:

$$A_0^2 = \frac{\left(A_{fr}^2 - \frac{\gamma_N}{\gamma_P} \Delta N_0\right)}{\left(1 + \frac{g\Delta N_0}{\gamma_P}\right)} \quad (5)$$

$$\phi_0 = \sin^{-1} \left\{ -\frac{\Delta\omega_{\text{inj}}}{k_c \sqrt{1 + \alpha^2}} \frac{A_0}{A_{\text{inj}}} \right\} - \tan^{-1} \alpha \quad (6)$$

The steady-state slave field and the phase offset between the slave and master laser and its boundary can be further used to derive an expression for detuning  $\Delta\omega_{\text{inj}}$ . However, computing the detuning value for a specific case is not possible unless the key parameters such as phase offset, linewidth enhancement factor, and injection strength can be extracted for that case.

### C. Small-Signal Analysis (Dynamic Solutions)

A detailed approach to find the small-signal solution of the rate equations expressed in (1) through (3) has been demonstrated in the literature [8], [10]. Based on this method, the absolute modulation frequency response function can be expressed as:

$$|H(\omega)|^2 = \left| \frac{\Delta A}{\Delta J} \right|^2 = \frac{|M|^2 (\omega^2 + Z^2)}{(C - A\omega^2)^2 + (B\omega - \omega^3)^2} \quad (7)$$

where the parametric terms  $A$ ,  $B$ ,  $C$ ,  $Z$ , and  $M$  can be defined and simplified as [10]:

$$\begin{aligned} A &= 2\eta \cos \phi_0 + \gamma_N + gA_0^2 \\ B &= \eta^2 + 2\eta \cos \phi_0 (gA_0^2 + \gamma_N) + gA_0^2 (\gamma_P - 2\eta \cos \phi_0) \\ C &= \eta^2 (\gamma_N + gA_0^2) - gA_0^2 (\gamma_P - 2\eta \cos \phi_0) Z \\ Z &= \eta (\alpha \sin \phi_0 - \cos \phi_0) \\ M &= \frac{g}{2} A_0 \end{aligned} \quad (8)$$

The injection strength is proportional to the coupling term and the field ratio as:

$$\eta = k_c \frac{A_{\text{inj}}}{A_0} = \frac{\eta_0}{R_{\text{FE}}} \quad (9)$$

where  $\eta_0$  is the maximum injection ratio and  $R_{\text{FE}} = A_0/A_{fr}$  is the slave field enhancement factor due to injection.  $\eta_0$  incorporates the external master to slave power ratio, the coupling efficiency between the slave and master laser, and efficiency of injected field entering the slave laser cavity due to facet reflectivity. At this point, the enhancement of the slave field is introduced as an additional term denoted as the field enhancement factor,  $R_{\text{FE}}$ , which takes into account the deviation of the slave steady-state field magnitude compared to its free-running value at high injection ratios and specific frequency detuning.

### D. Modulation Response Model

The modulation response model expressed in (7) and (8) can be used to simulate the modulation characteristics of an

injection-locking system in microwave domain. There are as many as eight fitting parameters involved in this model, and this large number of potentially unconstrained parameters allows for many possible solutions that will reduce confidence in extracted results. One of the goals of this paper is to reduce the number of fitting parameters through known free-running slave terms along with additional constraints on remaining injection-locking fitting terms. By doing so, the parametric terms  $A$ ,  $B$ ,  $C$ , and  $Z$  defined in (8) can be translated in terms of known free-running and injection-locked parameters. This reduces the number of fitting parameters and expresses the remaining parameters in terms of the injection-locking operating parameters, which then will be projected in the targeted relative modulation response function. Since the  $|M|^2$  term defined in (7) and (8) is independent of frequency, it can be cancelled in the relative modulation response form. The “ $A$ ” term in (8) is effectively a damping rate of the coupled oscillator as follows:

$$A = \gamma_{\text{slave}} + \gamma_{\text{th}} \quad (10)$$

The slave damping rate  $\gamma_{\text{slave}}$  is related to the free-running damping rate and scales with the field enhancement factor as:

$$\gamma_{\text{slave}} = gA_0^2 + \gamma_N = (\gamma_{\text{fr}} - \gamma_N)R_{\text{FE}}^2 + \gamma_N \quad (11)$$

where  $\gamma_{\text{fr}} = gA_{\text{fr}}^2 + \gamma_N$  is the free-running slave damping rate and  $\gamma_N$  is assumed to be independent of optical injection. The explicit relationship between the locked and free-running damping rates is a key feature of the current model and allows us to implicitly include nonlinear gain effects as explained below.  $\gamma_{\text{th}}$  is the threshold gain shift and appears as a damping component, resulting from moving the slave from its free-running condition. It is also related to the phase offset and injection strength such that:

$$\gamma_{\text{th}} = 2\eta \cos \phi_0 = 2 \left( \frac{\eta_0}{R_{\text{FE}}} \right) \cos \phi_0 = -g\Delta N_0 \quad (12)$$

Again it is necessary to note that the group velocity is implicit in the differential gain term “ $g$ ” everywhere in this derivation. Using (11) to substitute for the slave damping rate in (10) and rewriting the expression for “ $A$ ”, we have:

$$A = (\gamma_{\text{fr}} - \gamma_N)R_{\text{FE}}^2 + \gamma_N + \gamma_{\text{th}} \quad (13)$$

The second and most important term located in the denominator of the response function is “ $B$ ”, which corresponds to the overall resonance frequency of the system. Substituting the threshold gain shift  $\gamma_{\text{th}}$  in the “ $B$ ” term defined in (8) and rearranging yields:

$$B = \eta^2 + \gamma_{\text{th}} (gA_0^2 + \gamma_N) + gA_0^2 (\gamma_P - \gamma_{\text{th}}) \quad (14)$$

The second term in (14), which is related to the steady-state slave locked field and carrier lifetime as  $(gA_0^2 + \gamma_N)$ , effectively appears as a damping rate that can be directly linked to the slave damping rate,  $\gamma_{\text{slave}}$ . Using the definition in (11), this term can be replaced as following:

$$B = \eta^2 + \gamma_{\text{th}}\gamma_{\text{slave}} + gA_0^2 (\gamma_P - \gamma_{\text{th}}) \quad (15)$$

By multiplying both sides of the steady-state solution of the locked field found in (5) by the differential gain  $g$  and rearranging  $\gamma_P$  on the right hand side, yields:

$$gA_0^2 = \frac{gA_{\text{fr}}^2\gamma_P - \gamma_N g\Delta N_0}{\gamma_P + g\Delta N_0} \quad (16)$$

The first term in the numerator  $gA_{\text{fr}}^2\gamma_P$  corresponds to the free-running relaxation frequency squared  $\omega_r^2$ . Substituting the threshold gain shift defined in (12) allows (16) to be rewritten as:

$$gA_0^2 = \frac{\omega_r^2 + \gamma_N \gamma_{\text{th}}}{\gamma_P - \gamma_{\text{th}}} \quad (17)$$

Substituting (9), (11), and (17) into (15) and rearranging will give the following expression for the “ $B$ ” term:

$$B = (\omega_r^2 + \gamma_N \gamma_{\text{th}}) + \left( \frac{\eta_0}{R_{\text{FE}}} \right)^2 + \gamma_{\text{th}} [(\gamma_{\text{fr}} - \gamma_N) R_{\text{FE}}^2 + \gamma_N] \quad (18)$$

For the case of zero injection,  $\eta$  is zero and (18) is equal to the relaxation frequency squared of the slave laser,  $B = \omega_r^2$ , which simply represents the slave’s free-running operating condition. Similarly, by applying (9), (11), (12), and (17) into (8) and rearranging, “ $C$ ” can be simplified and expressed as:

$$C = \left( \frac{\eta_0}{R_{\text{FE}}} \right)^2 [(\gamma_{\text{fr}} - \gamma_N)R_{\text{FE}}^2 + \gamma_N] - (\omega_r^2 + \gamma_N \gamma_{\text{th}}) Z \quad (19)$$

The “ $Z$ ” term defined in (8) corresponds to the correlation between the detuning phase offset and linewidth enhancement factor and can be expressed as:

$$Z = \left( \frac{\eta_0}{R_{\text{FE}}} \right) (\alpha \sin \phi_0 - \cos \phi_0) \quad (20)$$

By manipulating (7) and applying the parametric terms expressed in (13) and (18)–(20), the relative modulation response function of a stably locked system can be expressed as:

$$\begin{aligned} |H_R|^2 &= \frac{|H(\omega)|^2}{|H(0)|^2} \\ &= \frac{\left(\frac{C}{Z}\right)^2 (\omega^2 + Z^2)}{(C - A\omega^2)^2 + (B\omega - \omega^3)^2} \frac{1}{(1 + (\omega/\gamma_c)^2)} \end{aligned} \quad (21)$$

It is important to note that the response function expressed in (21) has a cubic frequency dependence. Also, depending on the detuning condition, either the  $B$ -containing or  $C/A$ -containing terms in the denominator may have a dominant impact on the overall resonance frequency. The second term in the denominator accounts for the parasitic  $RC$  and carrier transport effects, where  $\gamma_c$  is considered as a free-running characteristic constant that can be extracted along with other free-running parameters.

### E. Identifying the Known Free-Running Operating Parameters

By taking into account all the terms in (21), one finds that eight fitting parameters including  $\omega_r$ ,  $\gamma_{\text{fr}}$ ,  $\gamma_N$ ,  $\gamma_{\text{th}}$ ,  $\eta_0$ ,  $R_{\text{FE}}$ ,  $Z$  and  $\gamma_c$  are needed for the simulation. All of the terms are expressed as angular frequencies except  $R_{\text{FE}}$ . Compared to previous research, this method represents a novel experimental

approach that allows an easy comparison of the relative magnitudes of the fitting parameters [8]. Since the model is comprised of multiple fitting parameters, there will be many solutions available that can fit the experimental data. Most of these possible solutions can be eliminated by introducing proper restrictions to the operating parameters during least-squares-fitting, such that they can vary only in an acceptable physical range. However, restrictions are not enough to reach a reasonable level of accuracy of the model unless it is combined with a reduction of the freely varying fitting parameters. Fortunately, some of these parameters can be extracted from the intrinsic free-running parameters, which can be determined from the slave laser operating characteristics.

The operating parameters of an uncoupled system (free-running slave) can be extracted from the standard and conventional modulation response model [15]:

$$|H_R|^2 = \frac{\omega_r^4}{(\omega_r^2 - \omega^2)^2 + \gamma_{fr}^2 \omega^2} \cdot \frac{1}{1 + (\omega/\gamma_c)^2} \quad (22)$$

This expression is used to fit the free-running modulation response and extract three of the fitting parameters: the free-running relaxation oscillation frequency  $\omega_r$ , the free-running damping rate  $\gamma_{fr}$ , and the parasitic roll-off induced by  $\gamma_c$ . These parameters are intrinsic characteristics of the slave laser and remain unchanged when the system is injection-locked. The other fitting parameter found in the free-running characteristics is the inverse differential carrier lifetime  $\gamma_N$ . This term can be directly extracted by plotting the known free-running damping rates as a function of the corresponding relaxation oscillation frequencies through the conventional expression  $\gamma_{fr} = K f_r^2 + \gamma_N$  [16]. Knowing the value of  $\gamma_N$  is beneficial, since it may have a significant impact on the high-frequency behavior of the system under modulation. Consequently, the number of fitting parameters can be reduced from eight to four by keeping the free-running terms constant during the simulation. Further constraints on the remaining fitting parameters are found by considering the theoretical limits of semiconductor physics.

### III. EXPERIMENTAL DATA AND CURVE-FITTING RESULTS

#### A. Experimental Setup and Data

Fig. 1 shows a schematic view of the injection-locking setup used in the experiment. The slave laser was a multimode QDash FP grown on an  $n^+$ -InP substrate. A detailed description of the slave laser structure is provided elsewhere [17]. The laser has a 4- $\mu\text{m}$ -wide ridge waveguide and 500- $\mu\text{m}$ -cleaved cavity length. The nominal emission wavelength of this FP device is around 1560 nm, and the threshold current was measured to be 45 mA at room temperature. The output power of the slave laser was carefully coupled into a single-mode polarization maintaining (PM) lensed fiber using a piezoelectric stage controller with sub-micron accuracy. The coupling efficiency of the slave laser into the PM lensed fiber was  $>40\%$ . The PM lensed fiber was connected to port 1 of a three-port PM circulator. The master laser used in this experiment was a tunable external cavity laser (New Focus 6200) with a single-mode PM fiber pigtail connected to the second arm of the circulator, port 2. A high resolution

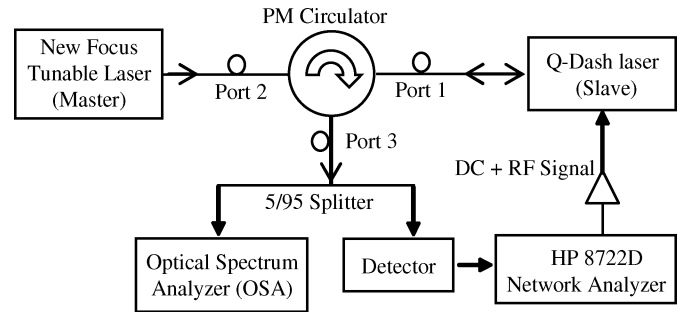


Fig. 1. Schematic view of the injection-locking QDash experimental setup.

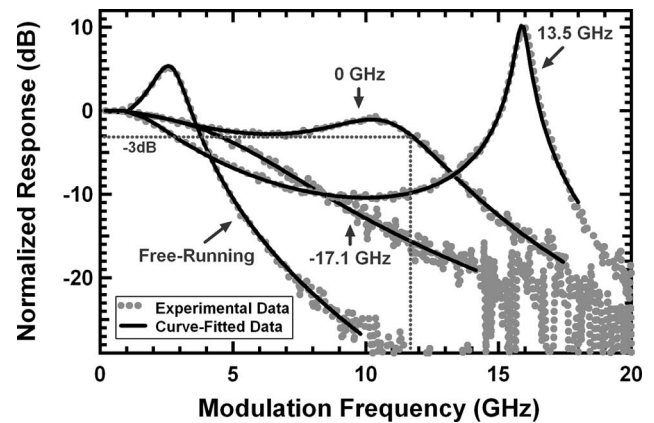


Fig. 2. Modulation responses of the free-running and the injection-locked laser under zero and extreme frequency detuning conditions.

(0.01 nm) optical spectrum analyzer (Ando AQ6317B) was connected to port 3 of the circulator to measure the detuning between the master and slave lasers, as well as to identify stably locked conditions.

Port 3 of the circulator was connected to a high-speed detector through which the relative modulation response ( $S_{21}$ ) was also measured using an HP 8722D network analyzer. The 5/95 beam splitter at port 3 of the circulator allowed to measure the modulation response of the injection-locked laser while simultaneously monitoring the detuning. This ensured that the desired detuning was stable throughout the experiment.

The modulation responses for various frequency detuning scenarios are provided in Fig. 2. The injected power provided by the master laser at the slave arm (port 1 of the circulator) and the total slave power at both facets was measured to be 3.5 and 4.7 dBm, respectively. The side mode suppression ratio (SMSR) for stable locking was taken to be 30 dB; using this criterion, stable locking was observed for detuning frequencies from 13.5 to  $-17.1$  GHz. At the zero frequency detuning condition, a 3-dB modulation bandwidth of 11.7 GHz was observed, which corresponds to a three-fold improvement relative to the free-running case. At the positive frequency detuning edge, the measured modulation response exhibits a large sag as well as a high-resonance peak. Due to significant damping, only a slight improvement in the modulation bandwidth is observed for the negative frequency cases.

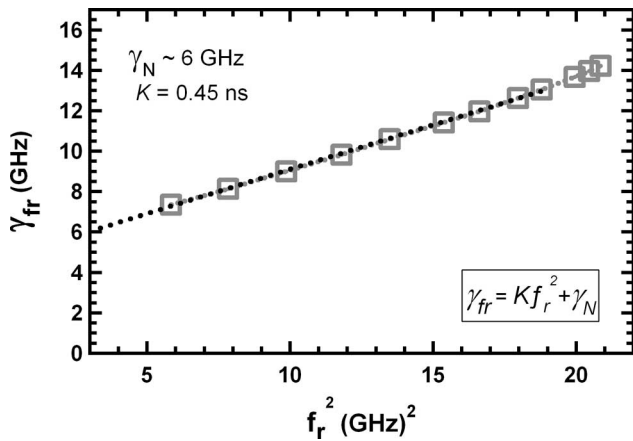


Fig. 3. Free-running damping factor as a function of the relaxation oscillation frequency squared.

### B. Determining the Free-Running Parameters and the Nonlinear Effects

As mentioned in the previous section, reducing the number of fitting parameters and applying reasonable constraints to the remaining fitting parameters improves the confidence in least-squares-fitting results by decreasing the number of possible solutions. In this case, the free-running slave parameters were obtained by fitting the free-running response curves measured for the QDash FP device to the conventional modulation response function expressed in (22). This examination of the free-running laser operating at a bias current of 60 mA yielded a free-running relaxation oscillation frequency of  $f_r = 2.7 \pm 0.02$  GHz, a free-running damping rate of  $\gamma_{fr} = 7.4 \pm 0.32$  GHz and a parasitic RC rate of  $\gamma_c = 67 \pm 0.4$  GHz. The error for the free-running values were measured based on a one standard deviation confidence interval and are observed to be less than 5% of their extracted values. In addition to these three values, the inverse differential carrier lifetime  $\gamma_N$  was found by plotting the free-running damping rate as a function of the relaxation oscillation frequency squared  $f_r^2$  as shown in Fig. 3. The corresponding value for  $\gamma_N$  is determined at the intersection of the plotted data with  $y$ -axis and was found to be approximately  $6 \pm 0.3$  GHz.

The  $K$ -factor, which is found from the slope of the curve in Fig. 3, is 0.45 ns and includes the effects of nonlinear gain compression in the usual manner [16], [18].

The impact of nonlinear gain on the free-running relaxation oscillation frequency can be studied through the following relation [19], [20]:

$$f_r^2 = \frac{CP_{out}}{1 + \varepsilon_p P_{out}} = \frac{CP_{out}}{1 + \frac{P_{out}}{P_{sat}}} \quad (23)$$

where  $\varepsilon_p$  is the gain compression factor related to the output power  $P_{out}$  and  $C$  is a fitting constant. The ratio of  $P_{out}/P_{sat}$  estimates the impact of gain compression factor at a given output power through the introduction of the saturation power  $P_{sat}$ . Based on the relation described in (23), the impact of nonlinear gain compression is incorporated into the injection-locking model through the free-running relaxation oscillation frequency, which will be kept constant during simulation. Fig. 4 shows the

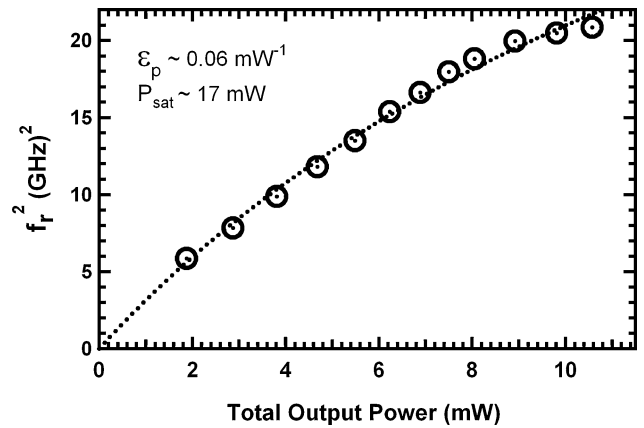


Fig. 4. Square of relaxation oscillation frequency versus the slave output power.

variation of the relaxation oscillation frequency squared as a function of the output power for the QDash device. Using (23) to fit the experimental data illustrated in Fig. 4 results in a saturation power of  $P_{sat} \sim 17$  mW, a gain compression factor of  $\varepsilon_p \sim 6 \times 10^{-2} \text{ mW}^{-1}$ , and a maximum free-running relaxation oscillation frequency of 7.6 GHz [20].

### C. Fitting Parameter Constraints

In order to reduce the number of possible solutions in this curve-fitting, it is necessary to put additional constraints on the four remaining fitting parameters,  $\gamma_{th}$ ,  $R_{FE}$ ,  $\eta_0$ , and  $Z$ , that are introduced by the injection-locking state. Due to the inter-relationship between these four parameters, constraining them reduces to restricting  $\phi_0$ ,  $\eta_0$ ,  $R_{FE}$ , and  $\alpha$ . This transformation is important because the  $\alpha$  of the investigated QDash FP laser has been found to change from  $\sim 1.0$  to 11 above threshold [21].

The constraints on the phase offset  $\phi_0$  are based on the allowed locking range through the threshold condition and considering (6). The result is that the phase offset varies between  $-\pi/2$  for positive frequency detuning up to  $\cot^{-1} \alpha$  for negative frequency detuning. At the extreme positive frequency detuning case, the phase offset between the master and slave should be  $-\pi/2$ . According to the phase condition at the positive frequency detuning edge, the value of the field enhancement factor  $R_{FE}$  should be 1, since the slave's steady-state field matches the free-running field due to the  $90^\circ$  phase offset between the master and slave. For all other possible values of detuning,  $R_{FE}$  is greater than 1.

The maximum injection ratio  $\eta_0$  can be extracted directly from known device characteristics and controllable parameters in the experimental setup. Using the fiber coupling efficiency  $\eta_c$ , the external power ratio  $R_{ext}$  (ratio of the master to the slave power measured outside of the slave's front facet), cavity length  $L$ , and front facet reflectance  $r$  of the FP slave laser, the maximum injection ratio is given as [22]:

$$\eta_0 = \frac{c}{2n_g L} \frac{(1 - r^2)}{r} \sqrt{\eta_c R_{ext}} \quad (24)$$

where  $c$  is the speed of light in free space and  $n_g$  is the optical group index. Using (24) and given a slave laser cavity length

of 0.05 cm, group index of 3.5, a mirror reflectivity of  $R = r^2 = 32\%$  for the cleaved facet, a coupling efficiency of 0.6 and an external power ratio of 1.5, the maximum injection ratio  $\eta_0$  was found to be 98 GHz. As the coupling efficiency was carefully maintained during these experiments, the maximum injection ratio was kept constant throughout the experiment. Since physically the threshold gain shift  $\gamma_{th}$  cannot exceed the photon decay rate  $\gamma_P$ , it is also important to verify that the calculated  $2\eta_0$  is less than  $\gamma_P$ , which in this case is 247 GHz.

The value of the linewidth enhancement factor for this device can be separately measured by using the injection-locking technique [20], [23]. The advantage of this method over other  $\alpha$ -measurement techniques is that no fitting parameters are required, which reduces the uncertainty of the measurement. This method takes advantage of the asymmetry in the stable locking region over a range of detuning on both the positive and negative side of the locked mode. Based on this technique and under the strong injection, the linewidth enhancement factor  $\alpha$  can be found using the following expression [23]:

$$\alpha = \sqrt{\left(\frac{\Delta f_{neg}}{\Delta f_{pos}}\right)^2 - 1} \quad (25)$$

where  $\Delta f_{neg}$  and  $\Delta f_{pos}$  correspond to the negative and positive frequency detuning ranges, which are determined by a SMSR limit of 30 dB. It is important to note that the value of SMSR is arbitrarily chosen depending on the limitations of the experiment. In this case, the SMSR is chosen large enough such that the weak side modes of the slave laser that are next to the injection-locked mode are always observable above the noise floor. Furthermore, for cases when the SMSR is chosen below 30 dB, these side modes may have a significant influence on the injection-locking stability boundary, causing an unreliable measurement for  $\alpha$  [24].

Using this method, the value of the linewidth enhancement factor can be measured through injection-locking boundaries for a specific applied bias current. Fig. 5 shows the variation of the linewidth enhancement factor as a function of applied bias current for this device, which increases from  $\sim 1.0$  to 11 as the applied bias current is increased from its threshold value to 90 mA. According to the results obtained from this measurement, the value of the linewidth enhancement factor is allowed to fluctuate as the detuning is adjusted based on the observation of large variations in the linewidth enhancement factor for this device, and attributed to the carrier density not being clearly clamped at threshold in the QDash FP laser under test [21]. This is one of the major differences in modeling the injection-locking behavior of the QDash laser.

#### D. Curve-Fitting Results

The parameters that were allowed to vary in the curve-fitting included the linewidth enhancement factor  $\alpha$ , phase offset between the master and slave laser  $\phi_0$  and field enhancement factor  $R_{FE}$ . All other fitting parameters are fixed and the curve-fitting constraints are summarized in Table I. The error for the parameters given in Table I was not carried forward into the least-squares-fitting of the coupled system as they were less than 5%

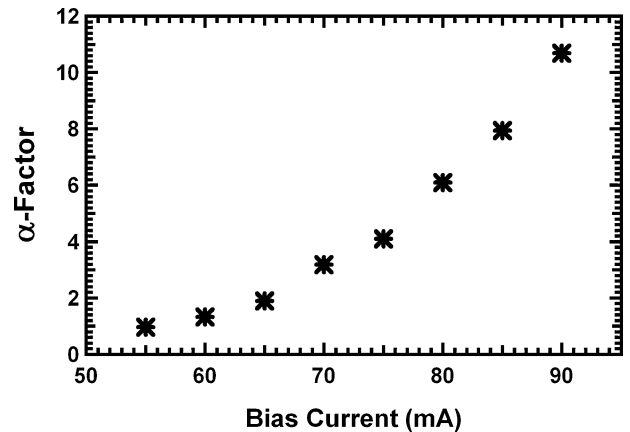


Fig. 5. Variation of the linewidth enhancement factor as a function of applied bias current in the QDash FP laser.

TABLE I  
FIXED FITTING PARAMETERS AND SUMMARY OF CONSTRAINTS USED IN THE LEAST-SQUARES-FITTING UNDER A BIAS CURRENT OF 60 mA

Fixed Fitting Parameters				
$f_r$ (GHz)	$\gamma_r$ (GHz)	$\gamma_n$ (GHz)	$\gamma_c$ (GHz)	$\eta_0$ (GHz)
$2.7 \pm 0.02$	$7.4 \pm 0.32$	$6 \pm 0.3$	$67 \pm 0.4$	98
Fitting Parameter Constraints				
$\alpha \geq 0$	$R_{FE} \geq 1$	$-\pi/2 \leq \phi_0 \leq \cot^{-1}\alpha$		

and thus considered to be negligible. Least-squares curve-fits of the experimental data using the modulation response function presented in (21) and parametric terms described in (13), (18)–(20) are shown in Fig. 2. The free-running device parameters were held constant in the modulation response function expressed in (21). The maximum injection ratio was constrained to be 98 GHz, as the coupling efficiency was carefully maintained during the measurements. The extracted phase shift was constrained between  $-\pi/2$  and  $\cot^{-1}\alpha$ . The field enhancement factor, phase offset, and linewidth enhancement factor were directly extracted through curve-fitting using (21), and the threshold gain shift was calculated for each detuning case by using (12). The operating parameters extracted through least-squares-fitting data collected for various measured detuning cases are presented in Table II. The error based on a one standard deviation confidence interval is also shown in Table II. The error associated with  $\alpha$ ,  $R_{FE}$ ,  $\gamma_{th}$ , and  $\phi_0$  are observed to be negligible for all detuning values away from the negative frequency detuning boundary. As the negative frequency detuning boundary is approached, the error increases for the extracted parameters. This is because, as shown in Fig. 2, the response becomes over-damped, which decreases the amount of information that can be extracted from a least-squares-fit of the corresponding modulation responses. Simulations using (21) show that as  $\phi_0$  approaches zero, changes to the values of  $\alpha$ ,  $R_{FE}$ , and  $\gamma_{th}$  result in only minor changes to the modulation response.

The calculated values for the threshold gain shift  $\gamma_{th}$  show an increase from positive to negative frequency detuning

TABLE II  
EXTRACTED INJECTION-LOCKING OPERATING PARAMETERS  
FROM LEAST-SQUARES-FITTING OF EXPERIMENTAL DATA WITH RESPONSE  
MODEL IN (21)

$\Delta f$ (GHz)	$\alpha$	$\phi_0$ (rad)	$R_{FE}$	$\gamma_{th}$ (GHz)
13.5	$1.59 \pm 0.07$	$-1.57 \pm 0.001$	$1.00 \pm 5 \times 10^{-4}$	$0.16 \pm 0.2$
11.0	$2.47 \pm 0.08$	$-1.48 \pm 0.002$	$1.06 \pm 8 \times 10^{-4}$	$16.8 \pm 0.4$
9.9	$2.46 \pm 0.08$	$-1.45 \pm 0.003$	$1.09 \pm 1 \times 10^{-3}$	$21.7 \pm 0.5$
6.1	$2.50 \pm 0.04$	$-1.37 \pm 0.003$	$1.24 \pm 1 \times 10^{-3}$	$31.5 \pm 0.4$
4.9	$2.55 \pm 0.04$	$-1.35 \pm 0.003$	$1.27 \pm 1 \times 10^{-3}$	$33.8 \pm 0.4$
0	$2.66 \pm 0.04$	$-1.21 \pm 0.006$	$1.40 \pm 2 \times 10^{-3}$	$49.4 \pm 0.7$
-3.7	$2.67 \pm 0.05$	$-1.09 \pm 0.01$	$1.48 \pm 5 \times 10^{-3}$	$61.2 \pm 1.3$
-8.6	$2.55 \pm 0.09$	$-0.95 \pm 0.03$	$1.52 \pm 1 \times 10^{-2}$	$75.0 \pm 2.9$
-13.5	$2.33 \pm 0.2$	$-0.58 \pm 0.2$	$1.60 \pm 5 \times 10^{-2}$	$102.5 \pm 8.4$
-15.9	$2.06 \pm 1.7$	$-0.17 \pm 0.2$	$1.79 \pm 2 \times 10^{-1}$	$107.4 \pm 21$
-17.1	$2.00 \pm 1.8$	$-0.03 \pm 0.2$	$1.80 \pm 2 \times 10^{-1}$	$108.8 \pm 23$

conditions. This trend is consistent with the induced threshold shift increasing as the injected and slave fields become more and more in phase from positive to negative frequency detuning.

The fitting results also show that the value of the field enhancement factor  $R_{FE}$  increases as the frequency detuning is reduced from the positive edge to the negative edge. This trend corresponds to theory describing an increase in the slave laser steady-state power under negative detuning conditions [22]. The extracted phase shift results are consistent with the theory stating that stable locking occurs for phase ranges from  $-\pi/2$  to  $\cot^{-1} \alpha$ . The extracted values of the linewidth enhancement factor for different detuning cases vary consistently within the expected range, which was measured separately for this device as reported in Fig. 5.

As also shown in Table II, the extracted values of the linewidth enhancement factor vary with detuning within the experimental error range. This leads to the conclusion that the linewidth enhancement factor can be manipulated by adjusting the detuning condition.

### E. Model-Based Analysis

With the validity of the modulation response model verified based on experimental data, it can be used to predict injection-locking behaviors for any FP slave laser once its free-running parameters are known.

By knowing the operating parameters of the system, it is then possible to predict the optimum operating limits of the device such as particular detuning frequencies and the maximum possible bandwidth. One key parameter having a prominent effect on the modulation response is the linewidth enhancement factor. The undesirable sag observed in the modulation response for the extreme positive frequency detuning, as shown experimentally in Fig. 2, can be removed by increasing the linewidth enhancement factor and keeping the same injection ratio.

In Fig. 6, the change in the modulation response under extreme positive frequency detuning due to a change in the linewidth enhancement factor is illustrated theoretically. At the positive frequency detuning edge, the phase off-

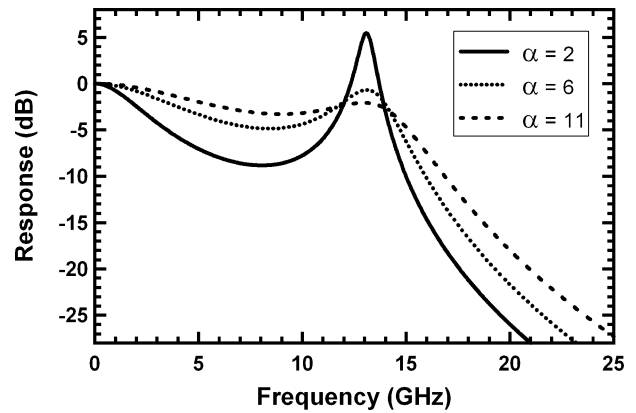


Fig. 6. Simulations of the modulation response function for various values of the linewidth enhancement factor.

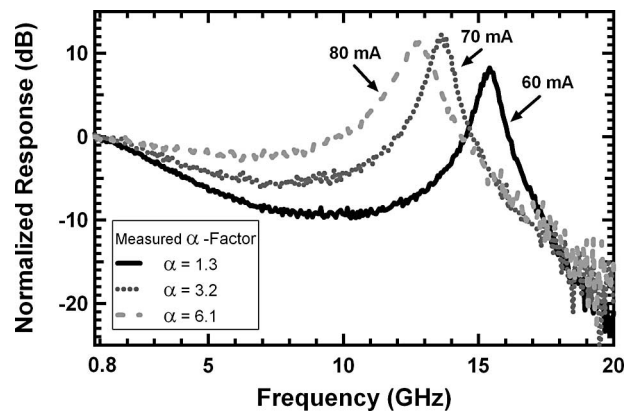


Fig. 7. Experimental observation of the varied sag as the linewidth enhancement factor is increased.

set is roughly  $-\pi/2$  causing the threshold gain shift to approach zero,  $\gamma_{th} \rightarrow 0$ , and the field enhancement becomes unity,  $R_{FE} = 1$ . The maximum injection ratio and the free-running fitting parameters are kept constant for all three cases. Values used in Fig. 6 were based on the extracted physical parameters for the injection-locked QDash FP device under test at extreme positive frequency detuning. The phase offset of  $\phi_0 \approx -\pi/2$  ( $-1.57$  rad), threshold gain shift of  $\gamma_{th} = 0.16$  GHz, and the field enhancement factor of  $R_{FE} = 1$  were kept constant for all three cases. Ideally, since the linewidth enhancement factor varies significantly in this device (1.0–11) based on the bias current, the sag in the modulation response should be removable assuming a high enough injection power is available to maintain a constant injection ratio. The significance of this observation is that because the highest relaxation oscillation frequency and hence the highest possible modulation bandwidth occur at the positive frequency detuning edge, removing the sag will achieve the highest possible modulation bandwidth for the injection-locked system. Fig. 7 experimentally demonstrates this trend, showing modulation response curves at the extreme positive frequency detuning edge for bias currents of 60, 70, and 80 mA and linewidth enhancement factor of 1.3, 3.2, and 6.1, respectively, as shown in Fig. 5. The sag is shown to be reduced (as the bias current, and correspondingly



the linewidth enhancement factor, is increased. Based on the theoretical model expressed in (21) and depending on how the  $B$ -containing and  $C/A$ -containing terms in the denominator interact, the sag reduces as their resonances detune from each other due to the change in the linewidth enhancement factor at different bias levels. The maximum injection ratio for the 60, 70, and 80 mA cases was calculated by (24) to be 103, 116, and 107 GHz, respectively. Note that although the peak frequency decreases as the bias current is increased, the magnitude of the peak remains relatively constant. The decrease in the observed relaxation oscillation frequency is likely due to the increased device heating as the bias current is increased, along with an increased cavity mode shift, which is driven by the linewidth enhancement factor as given in (4).

#### IV. CONCLUSION

Using a small-signal analysis of three coupled rate equations describing an injection-locked system, a novel modulation response function is demonstrated, which successfully models the key operating parameters of the system. It is shown that the model implicitly incorporates the nonlinear gain through the relaxation oscillation frequency and damping rate of the free-running slave laser. The impact of gain compression is evaluated for the slave device using a conventional technique that examines the variation of the square of the relaxation oscillation frequency as a function of output power. The presented model can be used to confidently extract microwave characteristics and operating parameters of the injection-locked system by reducing the number of fitting parameters and providing the acceptable physical constraints on the remaining fitting terms. This eliminates unwanted solutions resulting from curve-fitting and leads to a stronger confidence on the resultant extracted parameters.

Using this method, the characteristic parameters of an injection-locked system were extracted for a QDash FP slave laser. The validity of the model was examined based on the extracted value's correlation with theoretically expected values. The extracted parameters included the maximum injection ratio, linewidth enhancement factor, and threshold gain shift. As opposed to previous works, which primarily focused on analyzing experimental data in the spectral domain [4]–[7], this model demonstrates reliable curve-fitting results in the microwave domain. Finally, the model not only showed how the linewidth enhancement factor impacted the observed sag in the modulation response function, but also indicated how the sag can be virtually eliminated at higher bias current in a QDash FP laser.

The views expressed in this article are those of the author and do not reflect the official policy or position of the United States Air Force, Department of Defense, or the U.S. Government.

#### REFERENCES

- [1] F. Mogensén, H. Olesen, and G. Jacobsen, "FM noise suppression and linewidth reduction in an injection-locked semiconductor laser," *Electron. Lett.*, vol. 21, pp. 696–697, Aug. 1985.
- [2] N. Schunk and K. Petermann, "Noise analysis of injection-locked semiconductor injection lasers," *IEEE J. Quantum Electron.*, vol. QE-22, pp. 642–650, May 1986.
- [3] I. Petitbon, P. Gallion, G. Debarge, and C. Ghabran, "Locking bandwidth and relaxation oscillation of an injection-locked semiconductor laser," *IEEE J. Quantum Electron.*, vol. 24, no. 17, pp. 148–154, Aug. 1988.
- [4] T. B. Simpson, J. M. Liu, and A. Gavrielides, "Bandwidth enhancement and broadband noise reduction in injection-locked semiconductor lasers," *IEEE Photon. Technol. Lett.*, vol. 7, no. 7, pp. 709–711, Jul. 1995.
- [5] T. B. Simpson, J. M. Liu, and A. Gavrielides, "Small-signal analysis of modulation characteristics in a semiconductor laser subject to strong optical injection," *IEEE J. Quantum Electron.*, vol. 32, no. 8, pp. 1465–1468, Aug. 1996.
- [6] T. B. Simpson and J. M. Liu, "Enhanced modulation bandwidth in injection-locked semiconductor lasers," *IEEE Photon. Technol. Lett.*, vol. 9, no. 10, pp. 1322–1324, Oct. 1997.
- [7] J. M. Liu, H. F. Chen, X. J. Meng, and T. B. Simpson, "Modulation bandwidth, noise, and stability of a semiconductor laser subject to strong injection locking," *IEEE Photon. Technol. Lett.*, vol. 10, no. 10, pp. 1325–1327, Oct. 1997.
- [8] A. Murakami, K. Kawashima, and K. Atsuki, "Cavity resonance shift and bandwidth enhancement in semiconductor lasers with strong light injection," *IEEE J. Quantum Electron.*, vol. 39, no. 10, pp. 1196–1204, Oct. 2003.
- [9] L. Chrostowski, B. Faraji, W. Hofmann, M. C. Amann, S. Wiczorek, and W. W. Chow, "40 GHz Bandwidth and 64 GHz resonance frequency in injection-locked 1.55  $\mu\text{m}$  VCSELs," *IEEE J. Sel. Top. Quantum Electron.*, vol. 13, no. 5, pp. 1200–1208, Sep. 2007.
- [10] E. K. Lau, H. K. Sung, and M. C. Wu, "Frequency response enhancement of optical injection locked lasers," *IEEE J. Quantum Electron.*, vol. 44, no. 1, pp. 90–99, Jan. 2008.
- [11] E. K. Lau, X. Zhao, H. K. Sung, D. Parekh, C. Chang-Hasnain, and M. C. Wu, "Strong optical injection-locked semiconductor lasers demonstrating >100-GHz resonance frequencies and 80-GHz intrinsic bandwidths," *Opt. Exp.*, vol. 16, pp. 6609–6618, Apr. 2008.
- [12] R. Lang, "Injection locking properties of a semiconductor laser," *IEEE J. Quantum Electron.*, vol. QE-18, no. 6, pp. 976–983, Jun. 1982.
- [13] F. Mogensén, H. Olesen, and G. Jacobsen, "Locking conditions and stability properties for a semiconductor laser with external light injection," *IEEE J. Quantum Electron.*, vol. QE-21, no. 7, pp. 784–793, Jul. 1985.
- [14] C. H. Henry, N. A. Olsson, and N. K. Dutta, "Locking range and stability of injection locked 1.54  $\mu\text{m}$  InGaAsP semiconductor lasers," *IEEE J. Quantum Electron.*, vol. QE-21, no. 8, pp. 1152–1156, Aug. 1985.
- [15] P. Bhattacharya, D. Klotzkin, O. Qasimeh, W. D. Zhou, S. Krishna, and D. H. Zhu, "High-speed modulation and switching characteristics of In(Ga)As-Al(Ga)As self-organized quantum-dot lasers," *IEEE J. Sel. Top. Quantum Electron.*, vol. 6, no. 3, pp. 426–438, May/Jun. 2000.
- [16] R. Olshansky, P. Hill, V. Lanzisera, and W. Powazinik, "Frequency response of 1.3  $\mu\text{m}$  InGaAsP high speed semiconductor laser," *IEEE J. Quantum Electron.*, vol. QE-23, no. 9, pp. 1410–1418, Sep. 1987.
- [17] Y. Li, N. A. Naderi, V. Kovanis, and L. F. Lester, "Modulation response of an injection-locked 1550 nm quantum dash semiconductor laser," in *Proc. IEEE Lasers Electro-Opt. Soc. Conf.*, Oct. 21–25, 2007, pp. 498–499.
- [18] J. E. Bowers, "High speed semiconductor laser design and performance," *Solid-State Electron.*, vol. 30, pp. 1–11, 1987.
- [19] H. Su and L. F. Lester, "Dynamic properties of quantum dot distributed feedback lasers: High speed, linewidth and chirp," *J. Phys. D: Appl. Phys.*, vol. 38, pp. 2112–2118, Jun. 2005.
- [20] F. Grillot, N. A. Naderi, M. Pochet, C.-Y. Lin, and L. F. Lester, "Variation of the feedback sensitivity in a 1.55- $\mu\text{m}$  InAs/InP quantum dash Fabry-Perot semiconductor laser," *Appl. Phys. Lett.*, vol. 93, pp. 191108-1–191108-3, Nov. 2008.
- [21] F. Grillot, B. Dagens, J. G. Provost, H. Su, and L. F. Lester, "Gain compression and above threshold linewidth enhancement factor in 1.3- $\mu\text{m}$  InAs-GaAs quantum-dot lasers," *IEEE J. Quantum Electron.*, vol. 44, no. 10, pp. 946–951, Oct. 2008.
- [22] E. K. Lau, "High-speed modulation of optical injection-locked semiconductor lasers," Ph.D. dissertation, UC Berkeley, Dec. 2006.
- [23] G. Liu, X. Jin, and S. L. Chuang, "Measurement of linewidth enhancement factor of semiconductor lasers using an injection-locking technique," *IEEE Photon. Technol. Lett.*, vol. 13, no. 5, pp. 430–432, May 2001.
- [24] D. Dziak, A. J. Moscho, Y. Li, M. Fanto, V. Kovanis, J. Malowicki, and L. F. Lester, "Measurement of the linewidth enhancement factor of a 1550-nm injection-locked quantum dash laser," in *Proc. IEEE Lasers Electro-Opt. Soc. Conf.*, Oct. 21–25, 2007, pp. 433–434.

**Nader A. Naderi** (S'06) received the B.Sc. degree in applied physics from the Science University of Mashhad, Mashhad, Iran, and the M.Sc. degree (with distinction) in optoelectronics in 2007 from the University of New Mexico, Albuquerque, where he is currently working toward the Ph.D. degree at the Center for High Technology Materials.

He is currently with the University of New Mexico, where he is engaged in high-speed characteristics of semiconductor lasers. His current research interests include investigating the optical injection-locking technique on Fabry–Perot and DFB lasers and the impact of optical-feedback phenomenon on semiconductor lasers of various quantum structures.

**Mike Pochet** received the B.Sc. degree in electrical engineering from Virginia Polytechnic Institute and State University, Blacksburg, in 2001, and the M.Sc. degree in electrical engineering from the Air Force Institute of Technology (AFIT), Wright-Patterson Air Force Base, OH, in 2006. He is currently working toward the Ph.D. degree at the University of New Mexico, Albuquerque, through the Air Force's AFIT Civilian Institution Program.

His current research interests include high-speed semiconductor lasers.

**Frédéric Grillot** (S'01–M'06) was born in Versailles, France, on August 22, 1974. He received the M.Sc. degree in physics from Dijon University, Dijon, France, in 1999, and the Ph.D. degree in electrical engineering from Besançon University, Besançon, France, in 2003.

He was with the Optical Component Research Department, Alcatel. He studied the effects of the optical feedback in semiconductor lasers, and the impact this phenomenon has on optical communication systems for high-bit-rate transmissions. From May 2003 to August 2004, he was with the Institut d'Electronique Fondamentale, University of Paris-Sud, where he was engaged in integrated optics modeling and Si-based passive devices for optical interconnects and telecommunications. In September 2004, he was appointed to the Institut National des Sciences Appliquées de Rennes (INSA), Rennes, France, where he is currently an Associate Professor in the Materials and Nanotechnologies (MNT) Department. Since 2008, he has also been a Visiting Research Professor of electrical engineering at the University of New Mexico, Albuquerque, where he is leading research in optical science and optoelectronics at the Center for High Technology Materials. His current research interests include advanced laser diodes emitting at 1.55  $\mu\text{m}$  using new materials like quantum dots for low-cost applications.

Dr. Grillot is a Member of the IEEE-Lasers and Electro-Optics Society (LEOS) and the la Société Française d'Optique.

**Nathan B. Terry** received the B.Sc. and M.Sc. degrees in physics from Brigham Young University, Provo, UT, in 2000 and 2001, respectively, and the Ph.D. degree in applied physics from the Air Force Institute of Technology (AFIT), Wright-Patterson Air Force Base, OH, in 2007.

He is currently with the US Air Force Research Laboratory, Wright-Patterson Air Force Base (WPAFB), OH. He was engaged in numerical and experimental studies of Raman fiber lasers and Raman fiber amplifiers. His current research interests include high-speed semiconductor lasers.

**Vassilios Kovanis** received the B.S. degree in physics at the University of Athens, Athens, Greece, in 1983, the Graduate degree from Temple University, Philadelphia, PA, and the Ph.D. degree in condensed matter theory from the University of New Mexico, Albuquerque.

In September 1989, he joined the Non-Linear Optics Center, Air Force Weapons Laboratory, Kirtland Air Force Base, NM, and remained for the next 11 years, working on multiple projects of optical and electronic technologies. He also held research faculty positions with the Applied Mathematics and the Electrical Engineering Departments, University of New Mexico, and was a National Research Council Fellow between 1992 and 1994. He was also a Senior Research Scientist with corporate Research and Development Laboratories, Corning, Inc., Corning, NY, where he managed technical interactions with telecommunications system houses. He was also the Program Manager for next-generation photonic product development with BinOptics Corporation, Ithaca, NY. Between 2003 and 2005, he was a member of the faculty at the Applied Mathematics Department, Rochester Institute of Technology. In June 2005, he returned to the Air Force Research Laboratory, Wright-Patterson Air Force Base, OH, where he is currently with the Photonics Technologies Branch, Sensors Directorate. He has authored extensively on issues of optical injection locking, coherence collapse, optical coupling of semiconductor lasers as well in controlling, synchronizing, and communicating with chaotic waveforms.

**Luke F. Lester** (SM'00) received the B.S. degree in engineering physics and the Ph.D. degree in electrical engineering from Cornell University, Ithaca, NY, in 1984 and 1992, respectively.

He worked as an Engineer for the General Electric Electronics Laboratory, Syracuse, NY, where he worked on high-electron-mobility transistors for millimeter-wave applications. He is currently the Microelectronics Endowed Chair Professor in the Department of Electrical and Computer Engineering and an Associate Director of the Center for High Technology Materials, University of New Mexico (UNM), Albuquerque. He has over 20 years experience in III–V semiconductor materials and devices and was a Co-Founder and the Chief Technology Officer of Zia Laser, Inc., a startup company using quantum dot laser technology to develop products for communications and computer/microprocessor applications. He is the author or coauthor of 80 journal articles and more than 100 conference papers. His current research interests include quantum dot lasers, mode locking, injection locking, quantum dot solar cells, and III–V semiconductor processing.

Dr. Lester is an organizer of the Lasers and Electro-Optics Society (LEOS) conferences, workshops, and journals. He was an US Air Force Summer Faculty Fellow in 2006 and 2007. He was awarded the 1998 UNM School of Engineering Research Award, the 1994 Martin Marietta Manager's Award, and the 2007 UNM Electrical and Computer Engineering (ECE) Teaching Award.